**Smart Structures and Systems**, *Vol. 22, No. 6 (2018) 643-662*
DOI: https://doi.org/10.12989/sss.2018.22.6.643


# The effect of micro parameters of PFC software on the model calibration

M.R. Ajamzadeh[1], Vahab Sarfarazi[1], Hadi Haeri[*2] and H. Dehghani[3]

[1]*Department of Mining Engineering, Hamedan University of Technology, Hamedan, Iran*
[2]*Young Researchers and Elite Club, Bafgh Branch, Islamic Azad University, Bafgh, Iran*
[3]*Academic Member, Hamedan University of Technology, Hamedan, Iran*

*(Received July 10, 2018, Revised November 14, 2018, Accepted November 22, 2018)*

**Abstract.** One of the methods for investigation of mechanical behavior of materials is numerical simulation. For simulation, its need to model behavior is close to real condition. PFC is one of the rock mechanics software that needs calibration for models simulation. The calibration was performed based on simulation of unconfined compression test and Brazilian test. Indeed the micro parameter of models change so that the UCS and Brazilian test results in numerical simulation be close to experimental one. In this paper, the effect of four micro parameters has been investigated on the uniaxial compression test and Brazilian test. These micro parameters are friction angle, Accumulation factor, expansion coefficient and disc distance. The results show that these micro parameters affect the failure pattern in UCS and Brazilian test. Also compressive strength and tensile strength are controlled by failure pattern.

**Keywords:** PFC2D; friction angle; accumulation factor; expansion coefficient and disc distance

## 1. Introduction

There are two basics for using the versatile numerical methods to study the mechanical behavior of rocks i.e. continuum and dis-continuum (Jing 2003; Fu2005). The damage (failure or degradation) process in these brittle materials is the most important difference to be considered via continuum and dis-continuum mechanics known as direct or indirect methods (Potyondy and Cundall 2004). The indirect (continuum) approach usually takes into account the average material degradation based on the constitutive relations representing the micro-structural damage of the rock texture. On the other hand, the basic principal in the dis-continuum (direct) methods includes the separate units of the rock materials simulated as particles assemblies bonded together at their contact points where the breakage of the bonds in between the particles represent the damage process (Potyondy and Cundall 2004). The mechanical properties of discontinuous and heterogeneous rocks can be studied by considering them as granular materials with micro-mechanical behavior. Therefore, the conventional continuum methods may have some deficiencies in characterizing the micro-mechanical properties of rock materials. These deficiencies lead to the development of dis-continuum approaches such as discrete element method (DEM) as suggested and modified by Cundall and Strack 1979, Cundall 1987). Many researchers simulated the mechanical behavior of rocks by adopting the discrete element approach in form of two and three dimensional Particle Flow Codes (PFC2D and PFC3D) (Potyondy and Cundall 2004, Itasca 2004). A few experiments and simulations have been reported for the breakage analysis of concrete and rock specimens under different loadings (Mughieda and Alzo'ubi 2004, Wu *et al.* 2014, Zhao *et al.* 2013; Haeri *et al*. 2013, Lancaster *et al.* 2013, Ramadoss 2013, Pan *et al.* 2014, Noel and Soudki 2014, Oliveira and Leonel 2014, Mobasher *et al*. 2014, Wang *et al.* 2015, Gerges *et al.* 2015, Tiang *et al*. 2015, Lu *et al*. 2015, Liu *et al*. 2015, Wan Ibrahim *et al*. 2015, Haeri 2015, Haeri *et al*. 2015a, b, Lee and Chang 2015, Silva *et al*. 2015, Shuraim 2016, Sardemir 2016, Li *et al*. 2016, Sarfarazi *et al*. 2016, Haeri *et al.* 2016, Haeri and Sarfarazi 2016a,b, Akbas 2016, Rajabi 2016, Yaylac 2016, Fan *et al*. 2016, Mohammad 2016, Wang *et al*. 2017). The two dimensional Particle Flow Code (PFC2D) is based on the basic idea of treating the rock material as an assembly of particles bonded at specified points. This sophisticated software models the mechanical behavior of rock by considering the formation and interaction of microcracks developed within the particle assembly based on the Newtot's law of motion (Potyondy and Cundall 2004, Yan and Ji 2010). The most important application aspects of PFC are the assignment of model's microscopic parameters which are unknown and cannot be measured directly by experimental laboratory tests. These micromechanical properties are commonly back-calculated through the numerical calibrations against the macroscopic property values measured from laboratory experiments. The versatile iterative trial and error algorithm is usually adopted to determine the microscopic parameters of rock materials. A series of numerical simulations are conducted on the standard small-scale laboratory tests performed on the natural rock specimens so that the microscopic parameters can be reproduced and adequately approximate the measured macroscopic properties. The main macroscopic mechanical properties used for the calibration process

*Corresponding author, Assistant Professor
E-mail: h.haeri@bafgh-iau.ac.ir



ISSN: 1738-1584 (Print), 1738-1991 (Online)

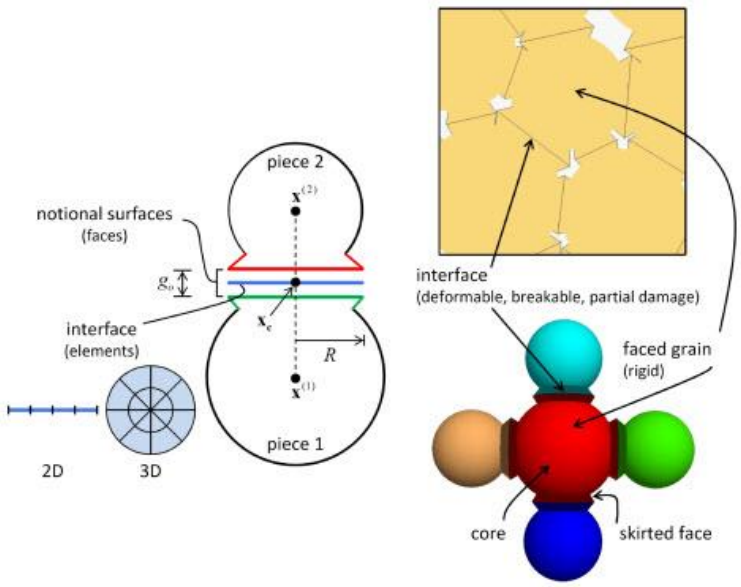


Fig. 1 Flat-joint contact (left) and flat-jointed material (right) [29]

include the unconfined compressive strength (UCS), Young's modulus and Poisson's ratio. However, this calibration process (as a priori step) has been studied extensively by different researchers in PFC2D (Huang 1999, Potyondy and Cundall 2004, Yang *et al.* 2006, Cho *et al.* 2007, Koyama and Jing 2007, Yoon 2007, Zhang *et al.* 2011, Zhang and Wong 2012, Ghazvinian *et al.* 2012, Bahaaddini *et al.* 2013, Sarfarazi *et al.* 2014, Sarfarazi 2016a, b, Potyondy, Cundall 2004, Li 2014, Potyondy 2015, Zhou 2016, Wang 2016, Wang and jacobs 2016, Oetomo 2016, Bahaaddini 2016, Yang 2016, Yang 2015, Oliaei 2015, Lin 2015, Turichshev 2015, Khazaei 2015, Bock 2015, Fan 2015, Zhang 2015, Wen 2016, Lee 2016, Vallejos 2016, Hofmann 2015, Li 2016, Mehranpour 2016, Yao 2016, Wang 2017, Ghazvinian 2017, Bahrani 2015, Hofmann 2016, Imani *et al.* 2017, Najigivi 2017, Khodayar and Nejati 2018, Nazerigivi *et al.* 2018, Kim *et al.* 2018). The highly non-linear local behavior of the bonded particles may cause some non-optimal microscopic parameters in the trial-and-error process. Some detailed studies were carried out on the microscopic properties calibration by Wang and Tonon (2009, 2010) using their DEM code. They conducted some sensitivity analyses and optimization process for calibration. The significant effects of the model size and micro-structural characteristics to be used in the numerical method on the simulated results are studied by Potyondy and Cundall (2004), Yang *et al.* (2006), Koyama and Jing (2007), Yoon (2007). They suggested that these effects shoukd be considering while applying the PFC simulation results. On another research, Koyama and Jing (2007) pointed out that a representative model should be used to study the relationship between microscopic parameters and macroscopic properties of rock materials for a reliable simulation of the real rock structures regardless of the numerical model size.

In this paper the effect of four micro parameters i.e., friction angle, Accumulation factor, Expansion coefficient and disc distance have been investigated on the uniaxial compression and Brazilian model calibration.

## 2. Calibration method

### *2.1 PFC software*

The discrete element codes such as PFC2D and PFC3D can be used to simulate many geo-mechanical problems through a discrete-element modeling framework. This geo-mechanical engineering package includes a computational engine augmented with a graphical user interface. The two and three dimensional discrete element models can be treated by PFC2d and PFC3D which simulate the movement and interaction of many finite-sized particles within particular particle assemblies. These particles are considered as rigid bodies having finite mass and can move (translate and/or rotate) independently. The interaction between these particles can be modeled using a pair-wise contacts approach provided by means of internal forces and moments. The contact mechanics is used to study the mechanical behavior of geo-mechanical problems based on the particle-interaction laws that update the internal forces and moments within the particle assembly.

The discrete-element method can compute the time evolution obtained through the explicit dynamic solution of the Newton's law of motion. A synthetic material can be modeled by PFC considering an assembly of rigid grains of granular and/or bonded materials interacting at contacts points (Potyondy and Cundall 2004). Flat joint model used in version 5 of PFC2D is one of the bonded contact models which is used to simulate a corresponding a piece of a body flat jointed material as shown in Fig. 1. The mechanical behavior of an interface in between the two notional surfaces connected rigidly to a piece of a rigid body can be efficiently simulated by a flat joint contact model. A flat

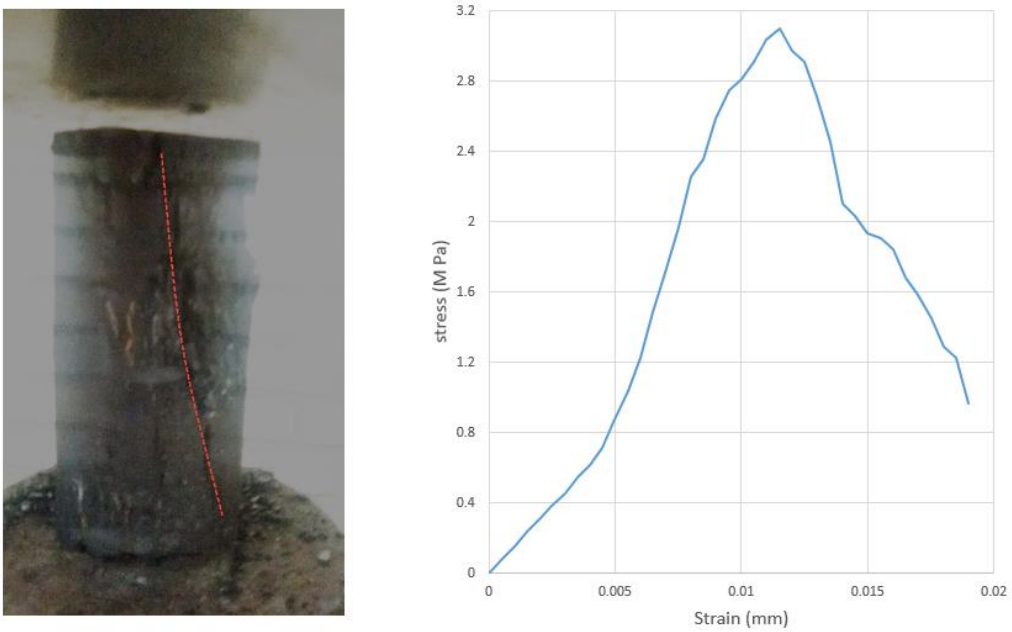


Fig. 2 stress-strain curve and failure pattern of coal rock

Fig. 3 Failure pattern in Brazilian test

jointed material includes the balls, clumps, or walls of bodies jointed by flat joint contacts. The effective contact surface for each body can be defined by the notional surfaces of the contacting pieces. These pieces may interact at each flat joint contact with the notional surfaces called faces defined as lines and discs for two and three dimensional bodies, respectively. The macroscopic behavior of the finite-size bonded or frictional interfaces that may sustain partial material damage considering the linear elastic behavior can be efficiently modeled by the flat-joint model used in PFC2D.

### *2.2 Experimental test*

Experimental samples are from Parvade Tabas coal mine situated from ease of Iran. These samples were subjected to Uniaxial compression test and Brazilian test. Stress-strain curve and failure pattern of coal rock was depicted in Fig. 2. Also Fig. 3 shows failure pattern in Brazilian test. Table 1 shows geometrical properties and mechanical properties of coal rock.

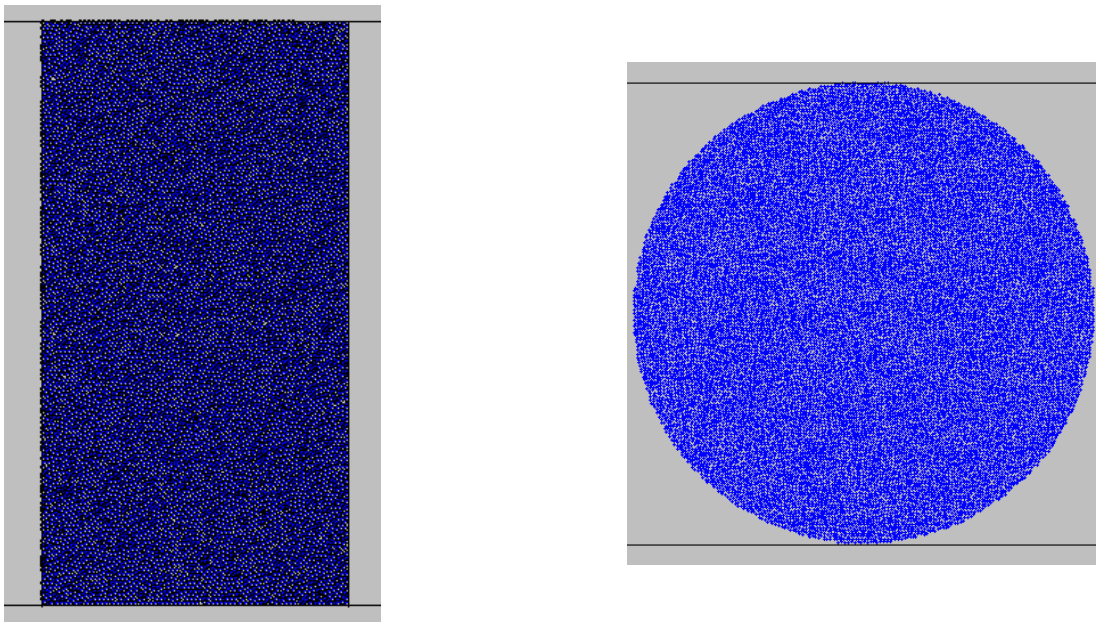

(a) (b)

Fig. 4 (a) the unconfined compression test and (b) Brazilian test

Table 1 geometrical properties and mechanical properties of coal rock

| Diameter [mm] | Length [mm] | Uniaxial compressive strength [MPa] | Tensile strength [MPa] |
|---|---|---|---|
| 55.4 | 108 | 3.1 | |
| 55.4 | 27 | ---- | 0.62 |

### *2.3 Coal rock calibration*

For calibration of coal rock, uniaxial compression test and Brazilian test were simulated by PFC2D version 5. Nineteen micro parameters should be change to get the best calibrated models (Table 2). These micro parameters are related to Model dimension, particle assembly and bonded particles contact properties. In this paper, only the effect of friction angle, Accumulation factor, Expansion coefficient and Particle distance on the model calibration has been studied.

#### *2.3.1 Numerical unconfined compressive test*

In PFC2D, the unconfined compression test can be simplified to a model of two moving walls compressing the particles assembly, as illustrated in Fig. 4(a). The walls were selected to be frictionless rigid plates. The tested specimen of assembly is 108 mm in height, 54 mm in width and consists of 14298 particles. A normal particle size distribution was used, with particle radii ranging from 0.6 mm to 1.2 mm. The bounds of the particle radii were chosen so as to have particles that are as small as possible, without compromising computational efficiency, and minimizing cod running time.

Table 2 Micro properties used for model calibration

| No | Micro properties | No | Micro properties |
|---|---|---|---|
| 1 | Particle distance | 11 | Model height |
| 2 | Elastic modulus (yang) | 12 | Model width |
| 3 | K-ratio | 13 | Expansion coefficient |
| 4 | Friction coefficient | 14 | Accumulation factor |
| 5 | Tensile strength | 15 | Density |
| 6 | Tensile strength standard deviation | 16 | Minimum diameter of particles |
| 7 | Compressive strength | 17 | Maximum diameter of particles |
| 8 | Compressive strength standard deviation | 18 | Material pressure |
| 9 | Friction angle | 19 | Material pressure changes |
| 10 | Porosity | 20 | |

#### *2.3.2 Brazilian test*

Brazilian test was used to calibrate the tensile strength of the specimen in PFC2D model (Fig. 4(b)). A normal particle size distribution was used, with particle radii ranging from 0.6 mm to 1.2 mm. The diameter of the Brazilian disk used in the numerical tests is 54 mm in diameter, and is made of 5615 particles. The disk was crushed by the lateral walls moved towards each other with a low speed of 0.016 m/s.

## 3. Result and discussion

### *3.1 The effect of friction angle on the model calibration*

In this study friction angle change in the values of: 0°, 10°, 15°, 20°, 30°, 40°, 45°, 50°, 60°, 70° and 80°.

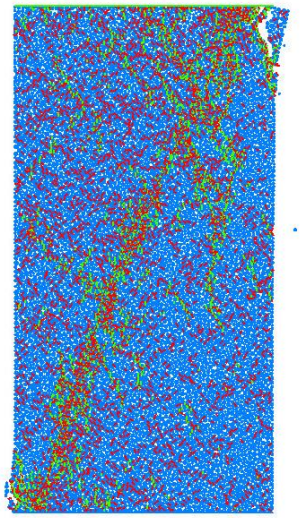

(a) 0°

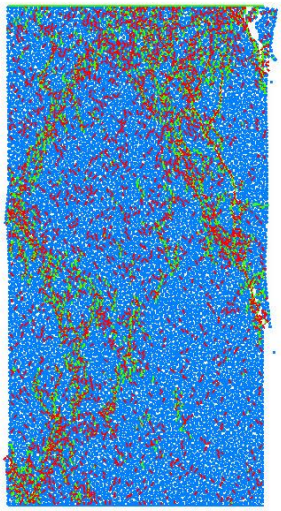

(b) 10°

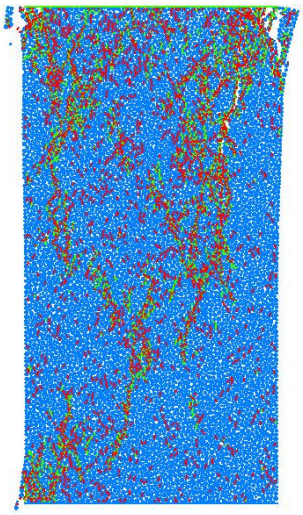

(c) 15°

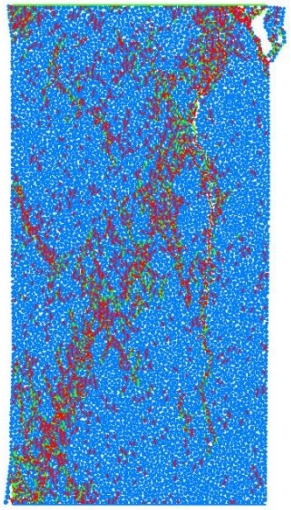

(d) 20°

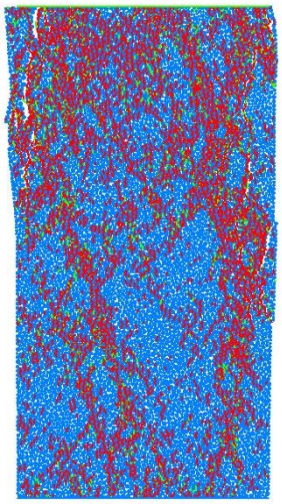

(e) 30°

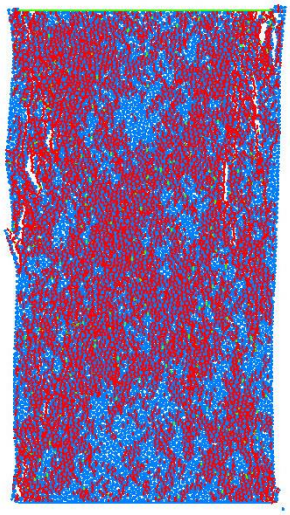

(f) 40°

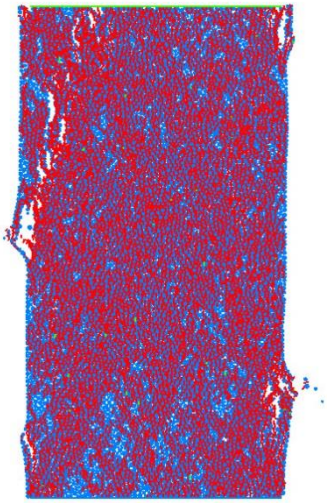

(g) 45°

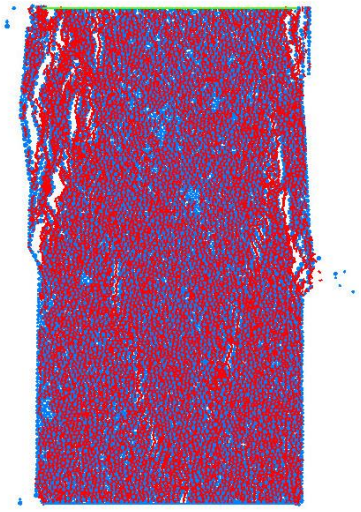

(h) 50°

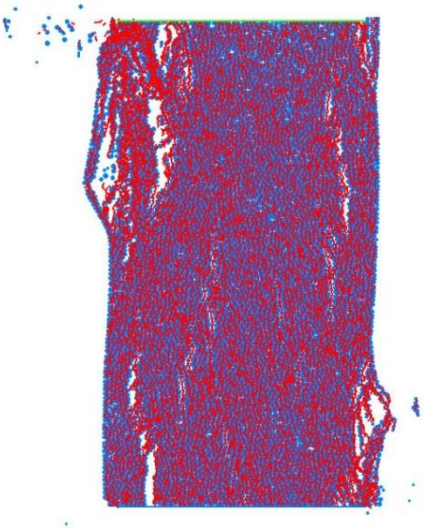

(i) 60°

Continued-

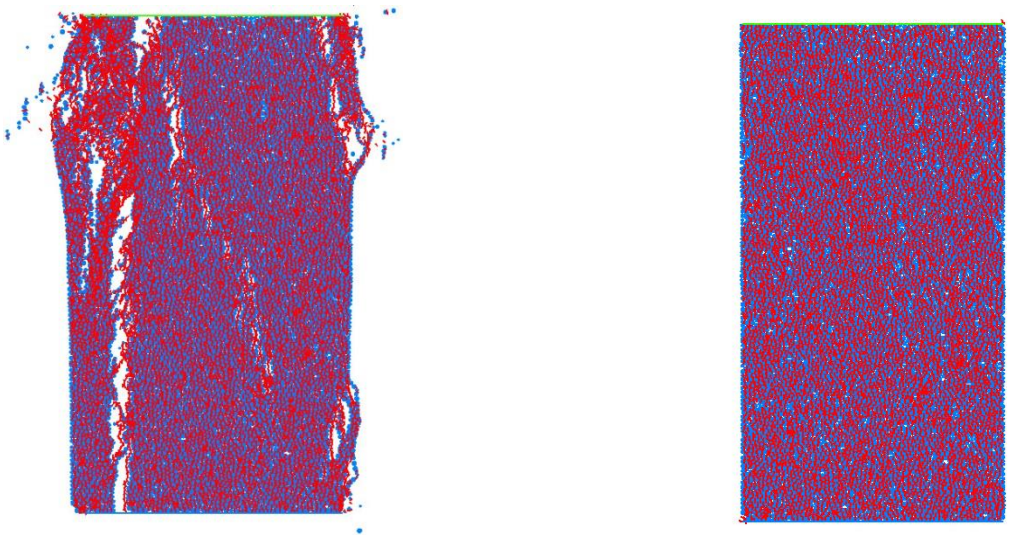

(j) (k)

Fig. 5 The effect of friction angle on the failure pattern in UCS test

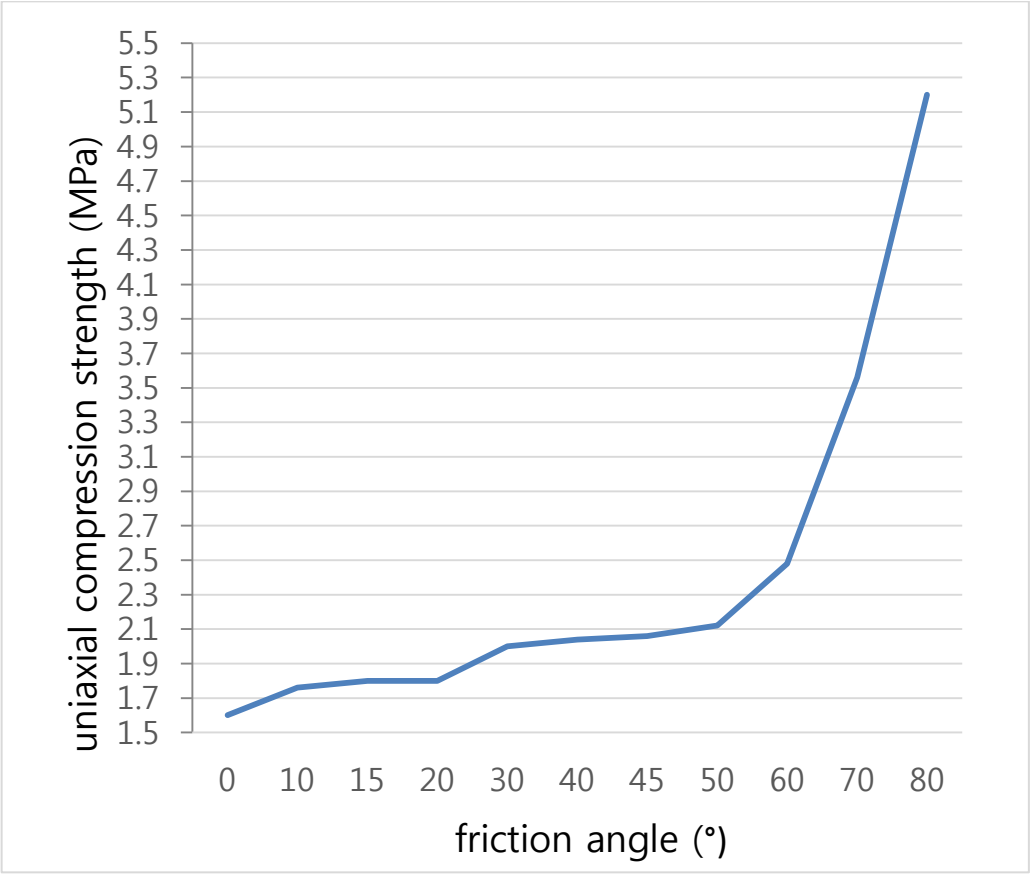


Fig. 6 The effect of friction angle on the uniaxial compression strength

Following section introduced the results of unconfined compression test calibration and Brazilian test calibration.

**a) The effect of friction angel on the UCS test outputs**

Fig. 5 shows the effect of friction angle on the failure pattern. Fig. 5 shows that the tensile cracks number increases by increasing the friction angle. When friction angle has low value, the failure surface angle is 45°. The splitting failure and sample rupture were occurred by increasing the friction angle. Fig. 6 shows the effect of friction angle on the uniaxian compression strength. The uniaxial compression strength is increased by increasing the friction angle. Its increase is graduated till 60° of friction

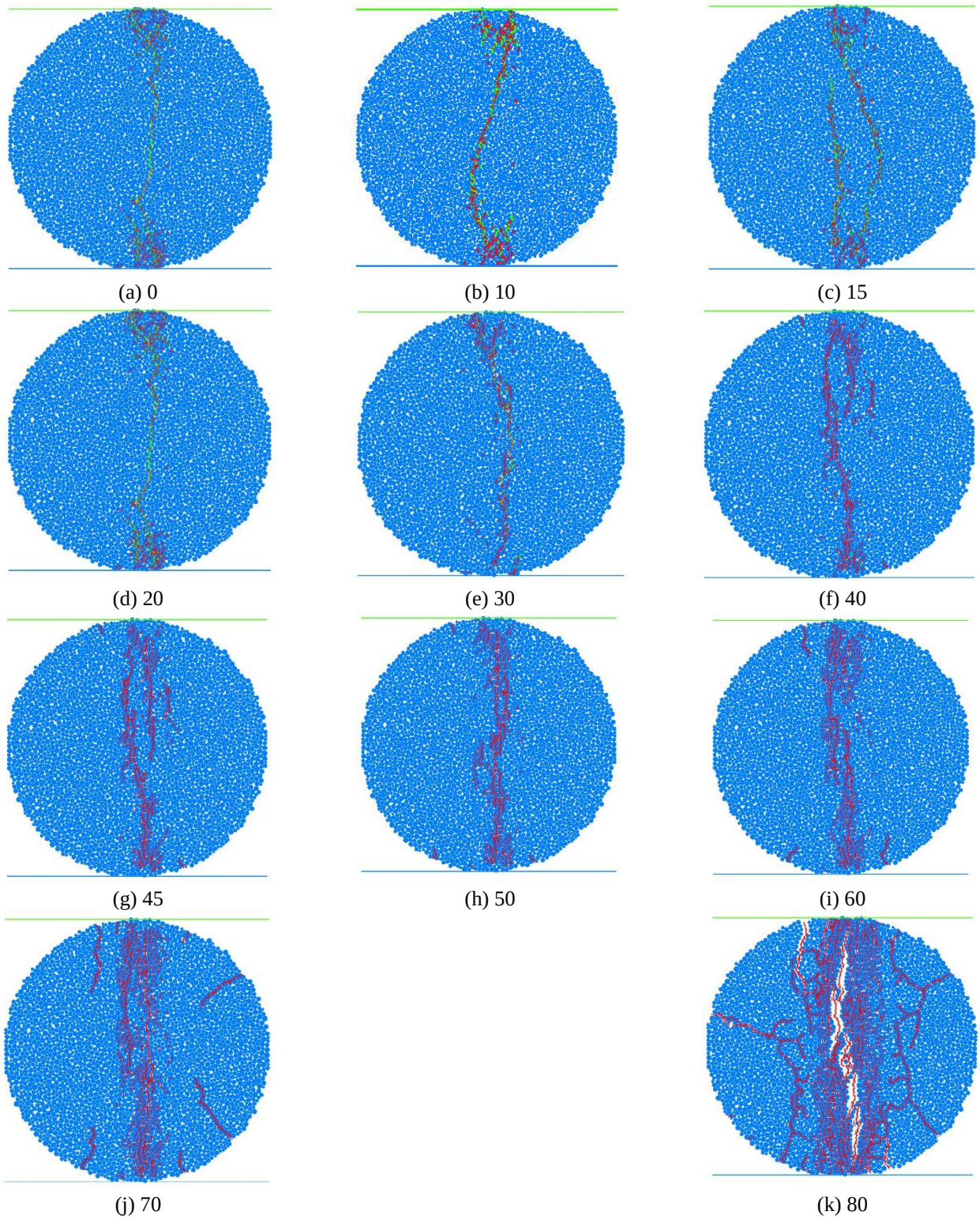


Fig. 7 The effect of friction angel on the Brazilian failure pattern

angle is reached. By increasing the friction angle more than 60°, the compressive strength is increases in higher rate.

By comparison between Fig. 5, Fig. 6 and Fig. 2 it can be concluded that the friction angel 20° was proper for model calibration. The output rendered by this friction angle is close to experimental one.

**b) The effect of friction angel on the Brazilian test outputs**

Figs. 7 and 8 show the effect of friction angel on the failure pattern and tensile strength, respectively. Fig. 7 shows that splitting failure change to multiple shear bands with increasing the friction angel. Also Fig. 8 shows that totally


Fig. 8 The effect of friction angel on the tensile strength

tensile strength is decreases by increasing the friction angle. By comparison between Figs. 7 and 8 and Fig. 3 it can be concluded that the friction angel of 20° was proper for model calibration. The output rendered by this friction angle is close to experimental one.

### *3.2 Accumulation factor*

In this study Accumulation coefficient change in following values: 0.1, 0.2, 0.3, 0.4, 0.5, 0.6 and 0.7. The following section introduced the results of unconfined compression test calibration and Brazilian test calibration.

**a) The effect of Accumulation factor on the UCS test outputs**

Fig. 9 shows the effect of accumulation factor on the compressive failure pattern. Fig. 9 shows that failure pattern changes from diametrical failure to several shear band with increasing the Accumulation coefficient. Fig. 10 shows the effect of accumulation factor on the UCS. Fig. 10 shows that totally compressive strength is decreases by increasing the Accumulation factor.. By comparison between Figs. 9 and 10 and Fig. 2 it can be concluded that the Accumulation coefficient of 0.7 was proper for model calibration. The output rendered by this Accumulation coefficient is close to experimental one.

**b) The effect of Accumulation factor on the Brazilian test outputs**

Fig. 11 shows the effect of accumulation factor on the tensile failure pattern. Fig. 11 shows that failure pattern was constant by increasing the Accumulation coefficient. Fig. 12 shows the effect of accumulation factor on the tensile strength. Fig. 12 shows that tensile strength is constant by increasing the Accumulation factor. It's to be note that only when the Accumulation coefficient was 0.7, the tensile strength was close to experimental one. Therefore the coefficient of 0.7 was chosen for model calibration.

### *3.3 Expansion coefficient*

In this study Expansion coefficient change in following values: 1, 1.2, 1.4, 1.6, 1.8, and 2. The values less than 1 and more than 2 lead to error in numerical results. The following section introduced the results of unconfined compression test calibration and Brazilian test calibration.

**a) The effect of accumulation factor on the UCS test outputs:**

Figs. 13 and 14 show the effect of Expansion coefficient on the failure pattern and UCS, respectively.

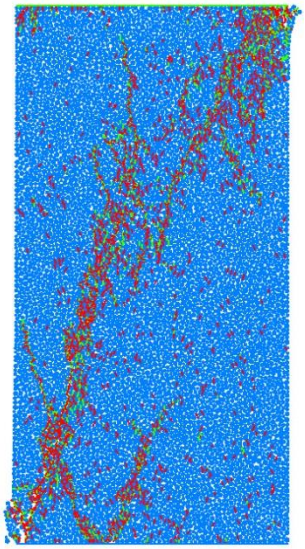

(a) 0.1

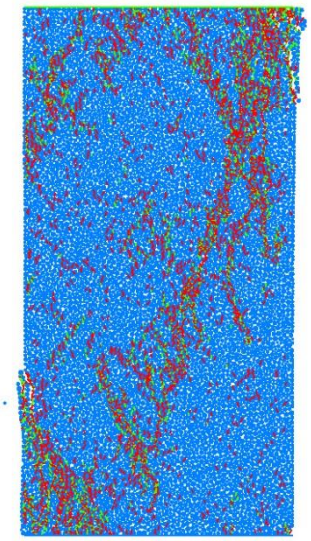

(b) 0.2

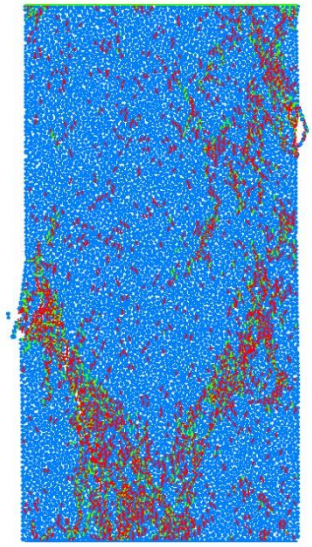

(c) 0.3

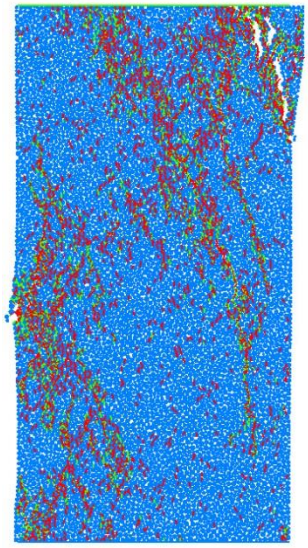

(d) 0.4

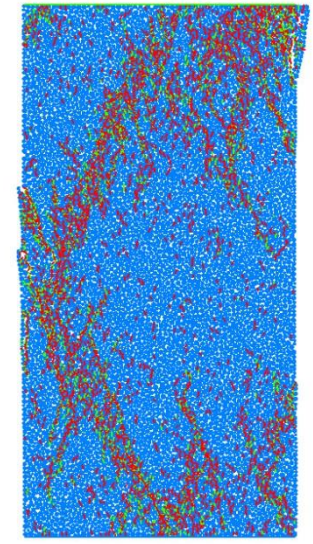

(e) 0.5

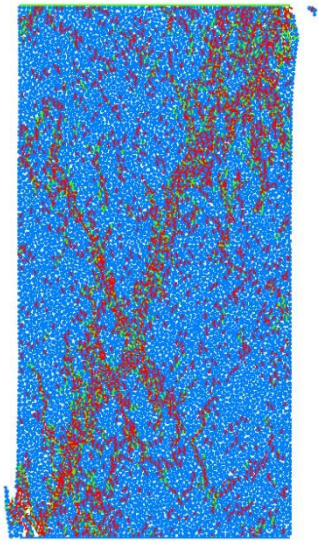

(f) 0.6

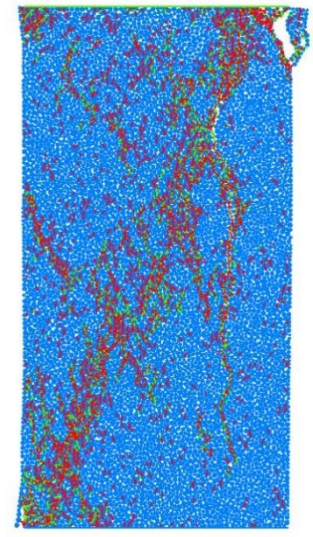

(g) 0.7

Fig. 9 The effect of Accumulation coefficient on the uniaxial failure pattern

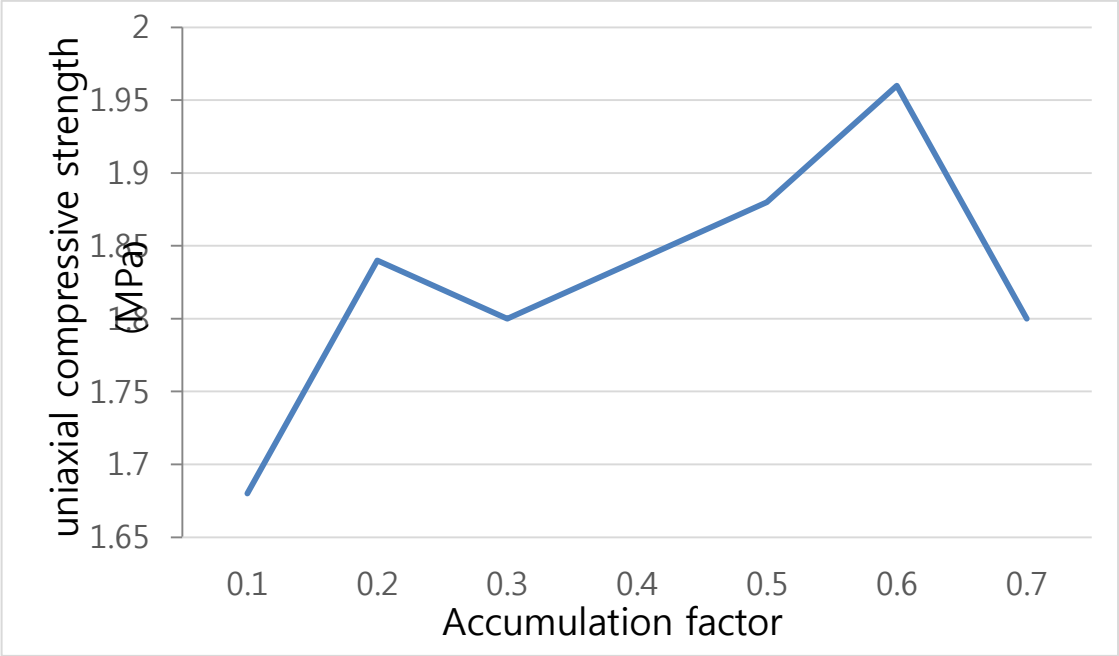


Fig. 10 The effect of Accumulation factor on the uniaxial compressive strength

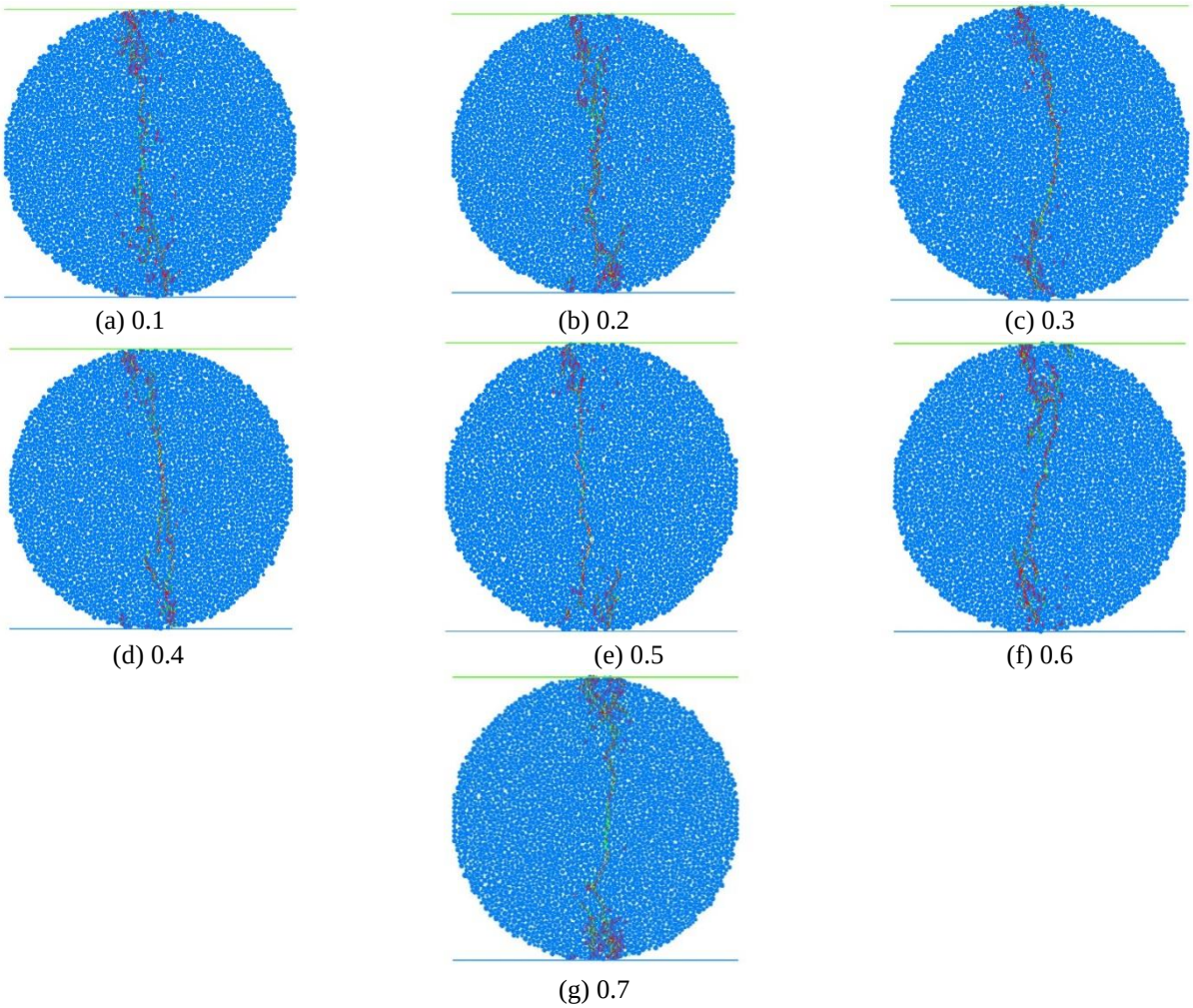


Fig. 11 The effect of Accumulation coefficient on the failure pattern

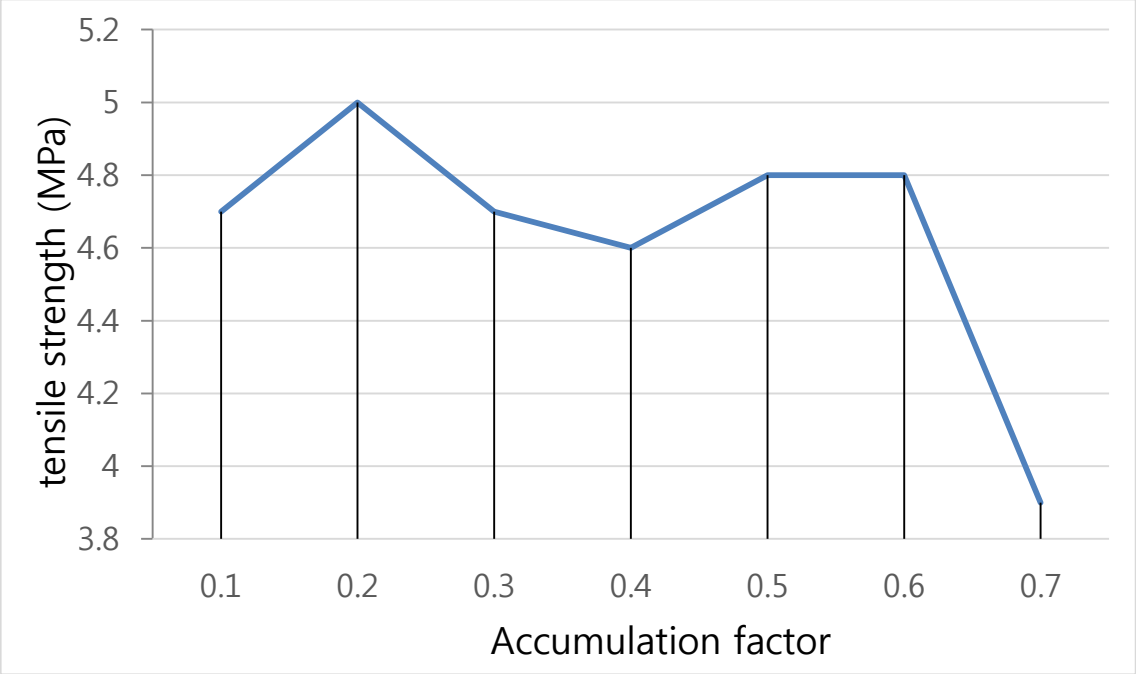


Fig. 12 The effect of Accumulation factor on the tensile strength

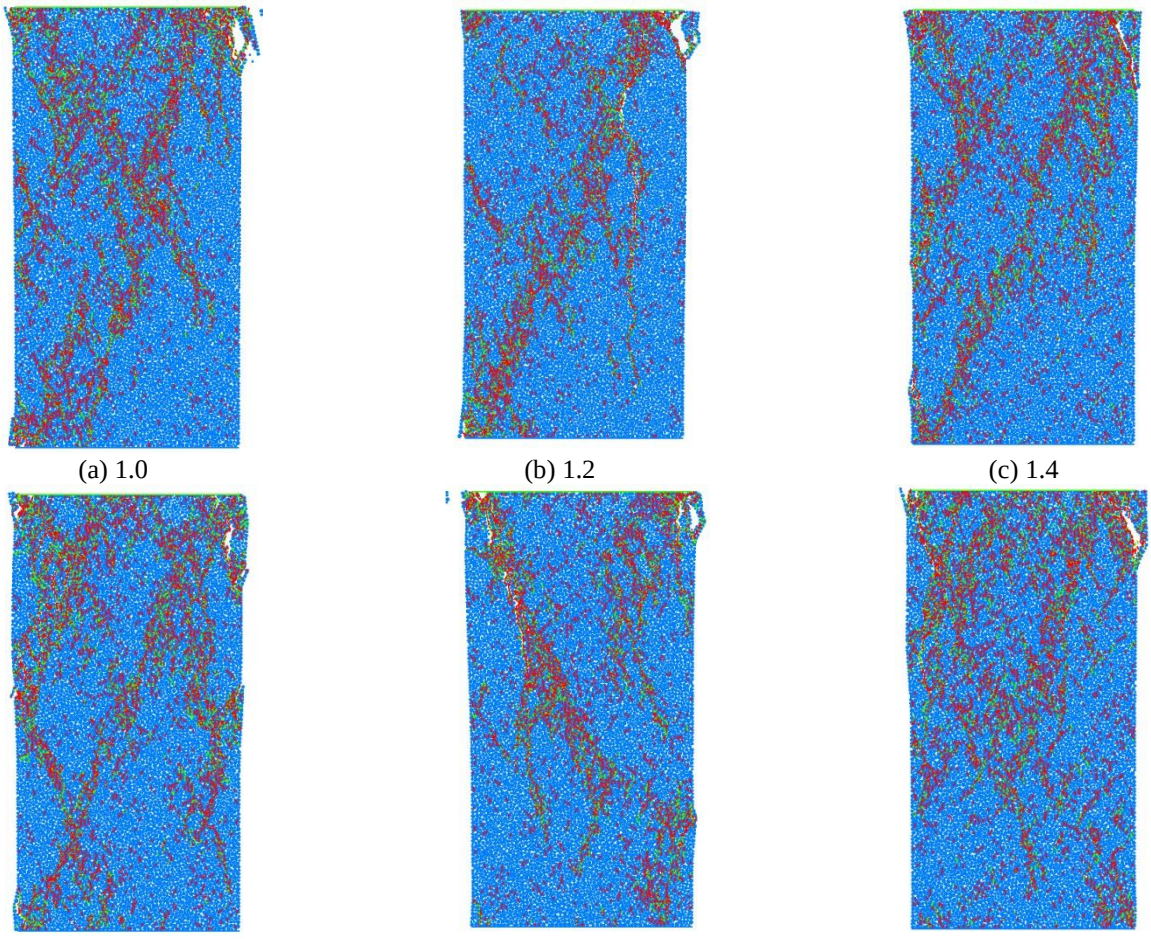

(a) 1.0 (b) 1.2 (c) 1.4

(d) 1.6 (e) 1.8 (f) 2.0

Fig. 13 The effect of Expansion coefficient on the failure pattern

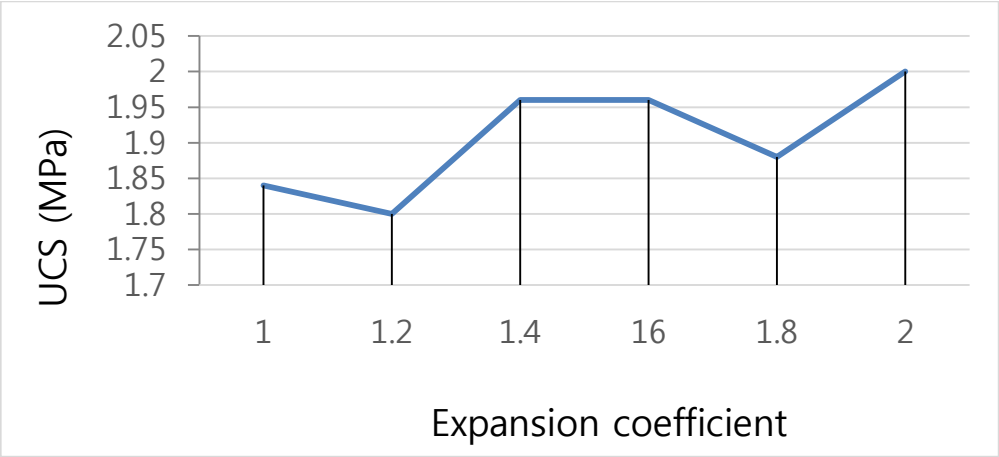


Fig. 14 The effect of Expansion coefficient on the UCS

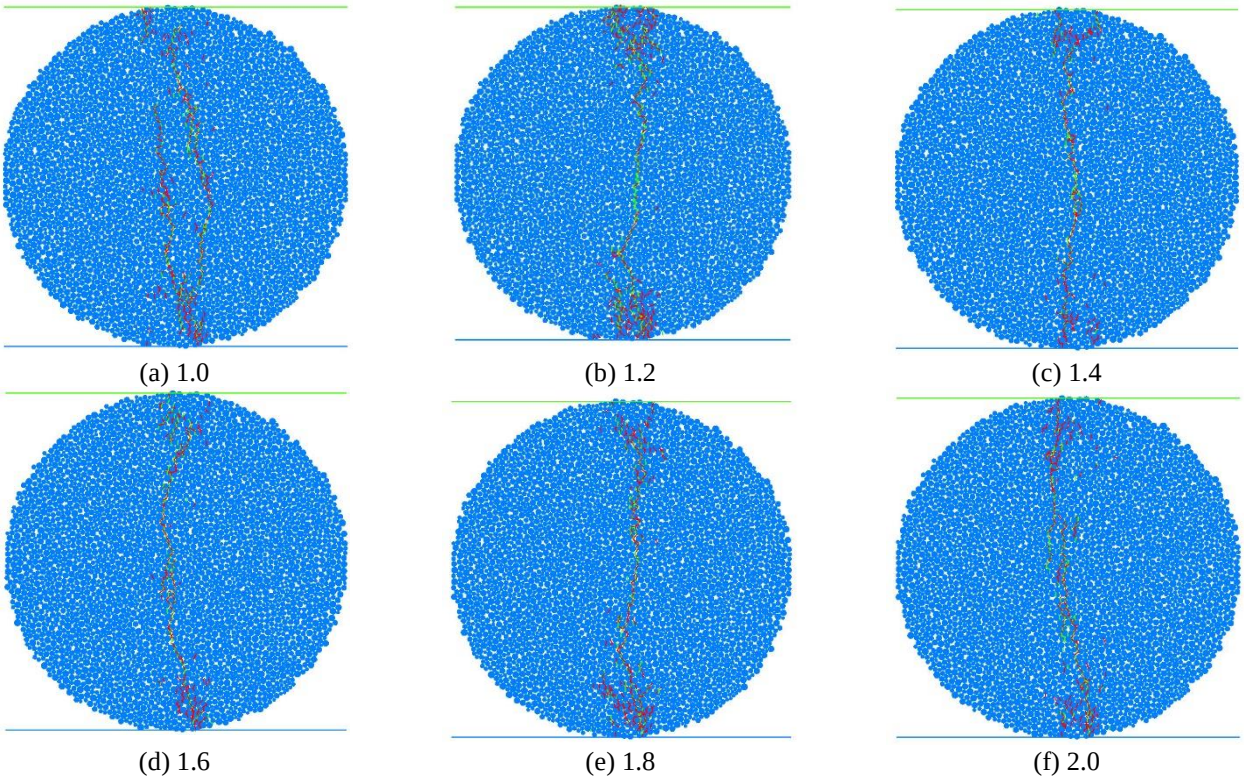

(a) 1.0 (b) 1.2 (c) 1.4

(d) 1.6 (e) 1.8 (f) 2.0

Fig. 15 The effect of Expansion coefficient on the Brazilian failure pattern

Fig. 13 shows that failure pattern changes from diametrical to several shear band with increasing the Expansion coefficient. Fig. 14 shows that unconfined compression strength was increased by increasing the Expansion coefficient. Its to be note that only when the Expansion coefficient was 1.2, the compressive strength and failure pattern were close to experimental one. Therefore the coefficient of 1.2 was chosen for model calibration.

**b) The effect of expansion coefficient on the brazilian test outputs**

Fig. 15 shows the effect of accumulation factor on the tensile failure pattern. Fig. 15 shows that failure pattern was constant by increasing the expansion coefficient. Only when the Expansion coefficient was equal to 1, the failure pattern are accomplished by several shear band. Fig. 16 shows the effect of expansion coefficient on the tensile strength. Fig. 16 shows that tensile strength is increased by increasing the Expansion coefficient. Its to be note that only when the Expansion coefficient was 1.2, the tensile strength and failure pattern was close to experimental one. Therefore the coefficient of 1.2 was chosen for model calibration.

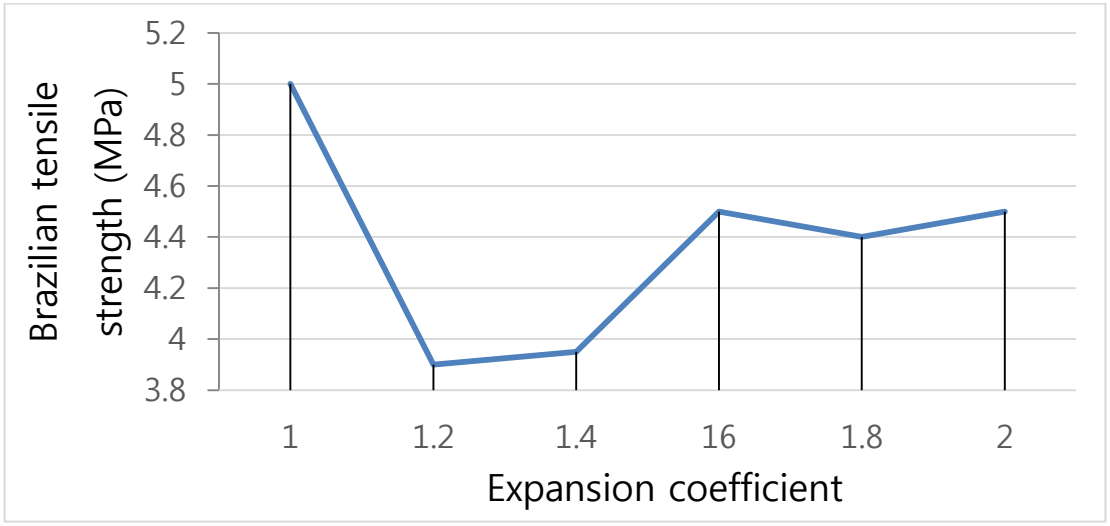


Fig. 16 The effect of Expansion coefficient on the Brazilian tensile strength

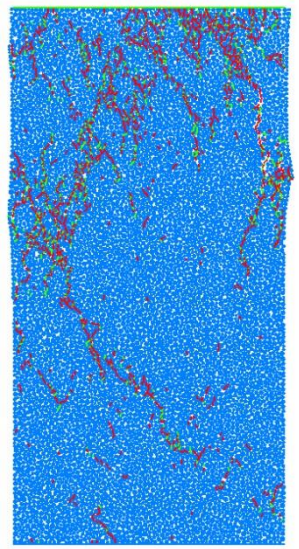

(a) 0.1

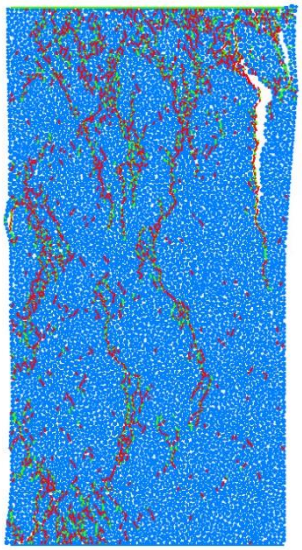

(b) 0.2

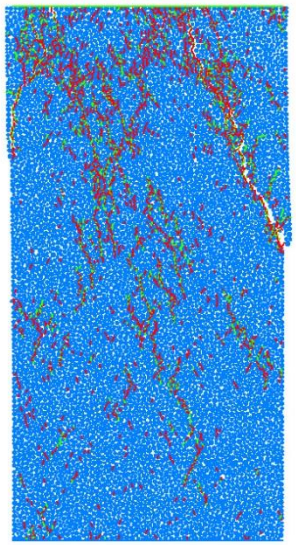

(c) 0.3

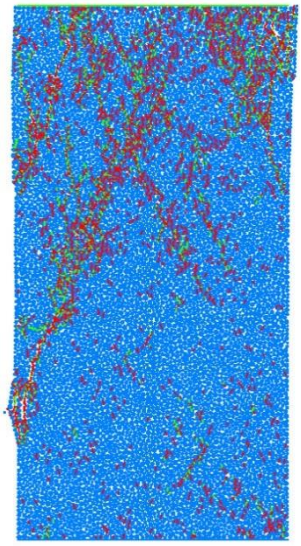

(d) 0.4

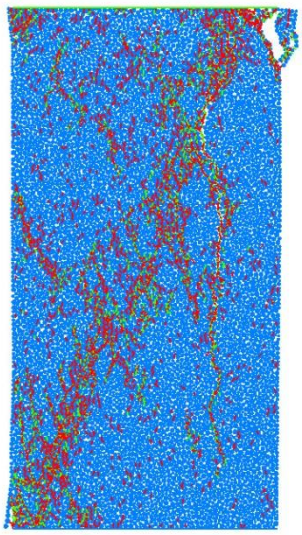

(e) 0.5

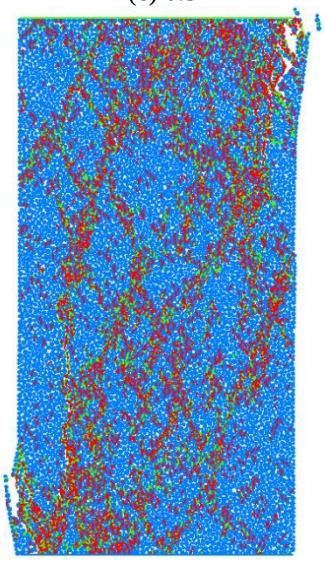

(f) 0.6

Continued-

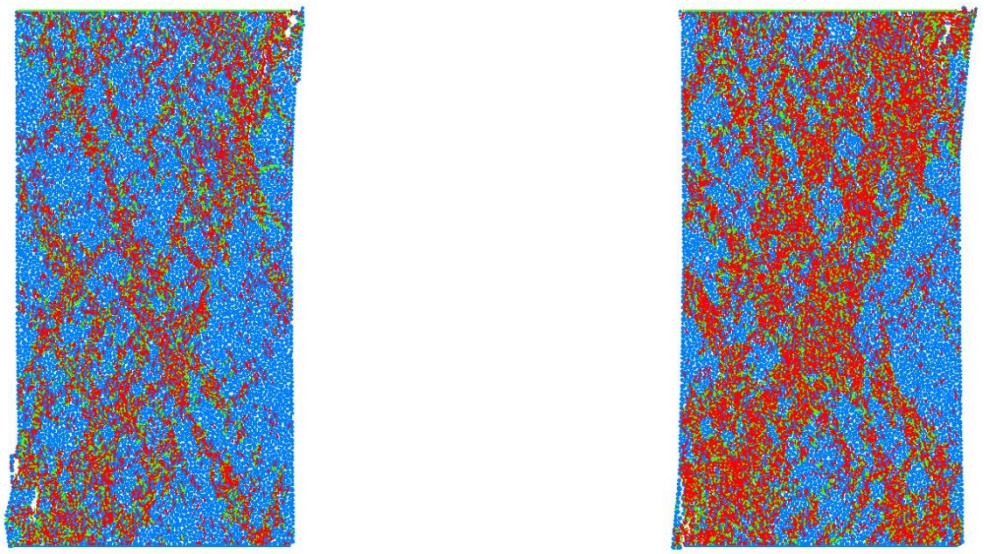

(g) 0.7 (h) 0.8

Fig. 17 The effect of Particle distance on the failure pattern

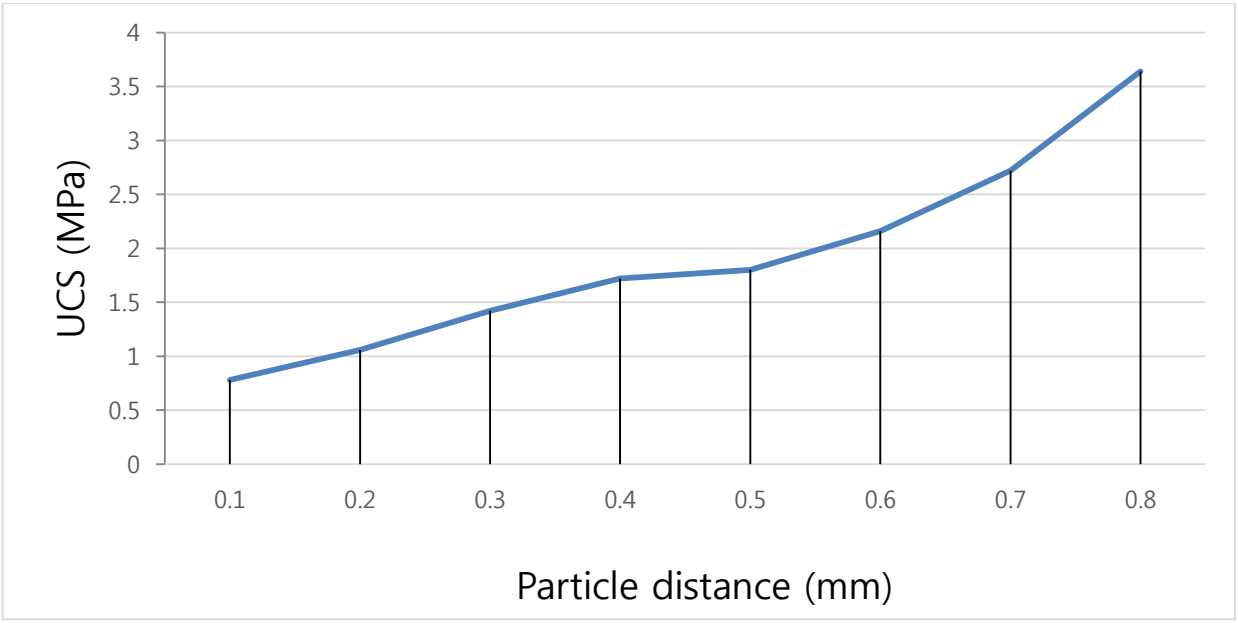


Fig. 18 The effect of Particle distance on the UCS

### *3.4 disc distance*

In this study Particle distance change in following values: 0.1 mm, 0.2 mm, 0.3 mm, 0.4 mm, 0.5 mm, 0.6 mm, 0.7 mm and 0.8 mm. The following section introduced the results of unconfined compression test calibration and Brazilian test calibration.

**a)The effect of disc distance on the UCS test outputs**

Fig. 17 shows the effect of Particle distance on the failure pattern. When Particle distance is less than 0.5, several shear band distributed in the model. When Particle distance is 0.5, diametrical failure occurred in the model. When Particle distance is more than 0.5, number of tensile cracks was increased and several shear bands distributed in the model transversely. Fig. 18 shows the effect of Particle distance on the UCS. Fig. 18 shows that uniaxial compressive strength was increased by increasing the Particle distance. Its to be note that only when Particle distance was 0.5, the UCS and failure pattern was close to experimental one (Fig. 2). Therefore the coefficient of 0.5 was chosen for model calibration.

**b) The effect of disc distance on the brazilian test outputs**

Fig. 19 shows the effect of Particle distance on the failure pattern. Failure pattern was constant with increasing the Particle distance. Fig. 20 shows the effect of Particle

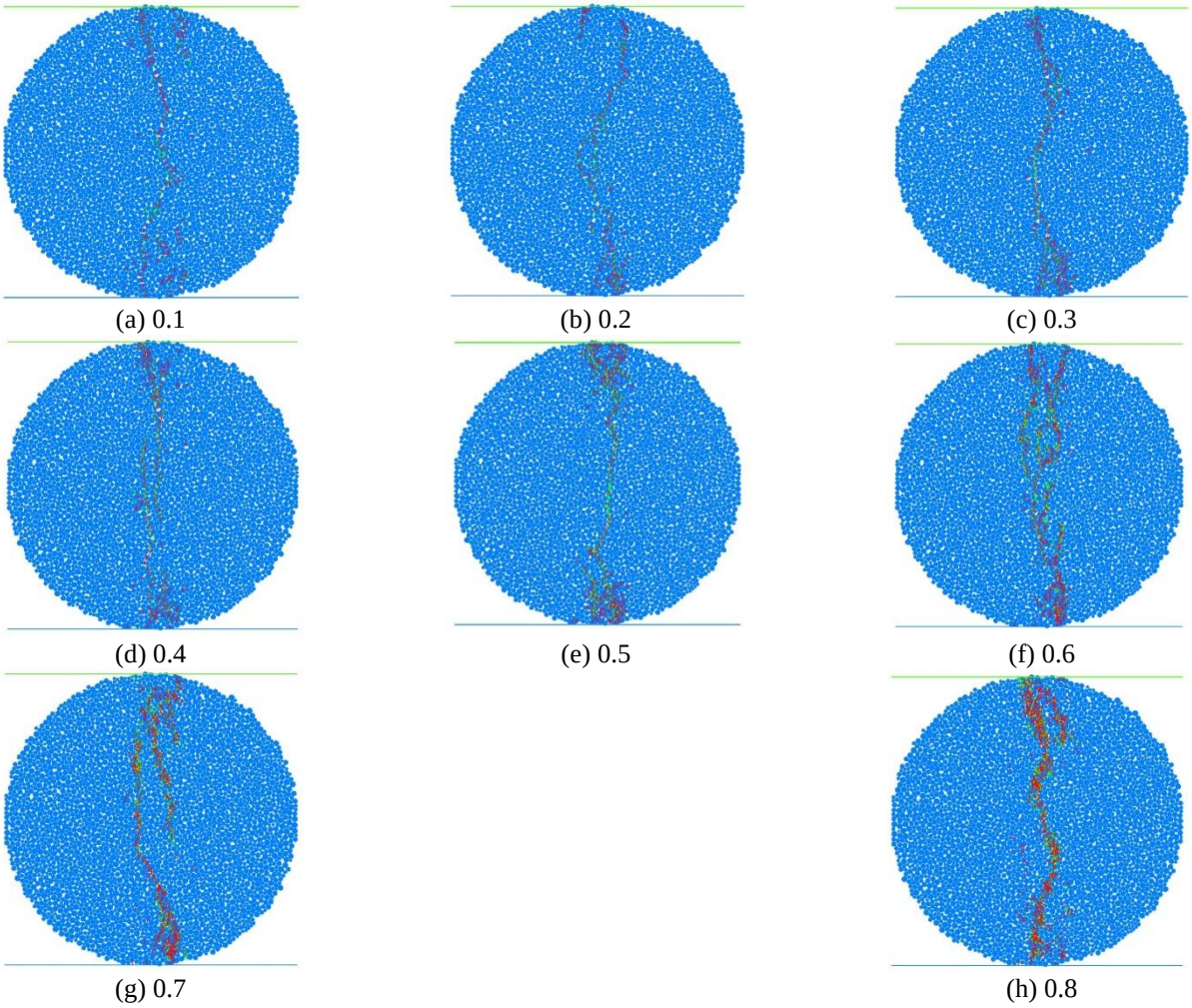

(a) 0.1 (b) 0.2 (c) 0.3

(d) 0.4 (e) 0.5 (f) 0.6

(g) 0.7 (h) 0.8

Fig. 19 The effect of Particle distance on the failure pattern

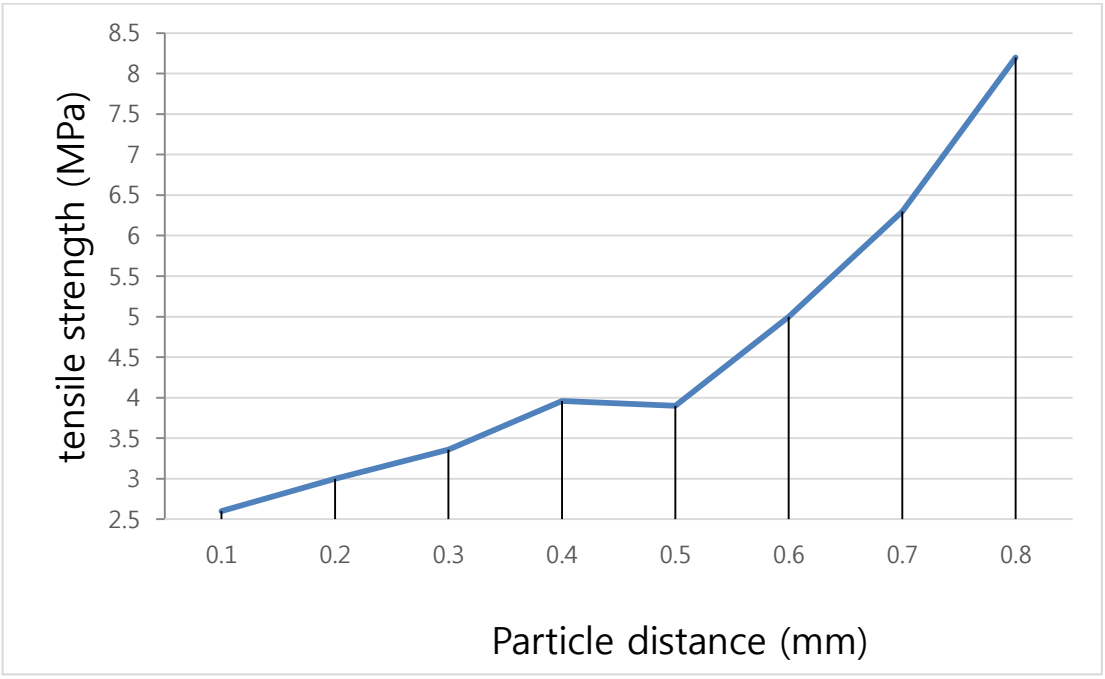


Fig. 20 The effect of Particle distance on the tensile strength

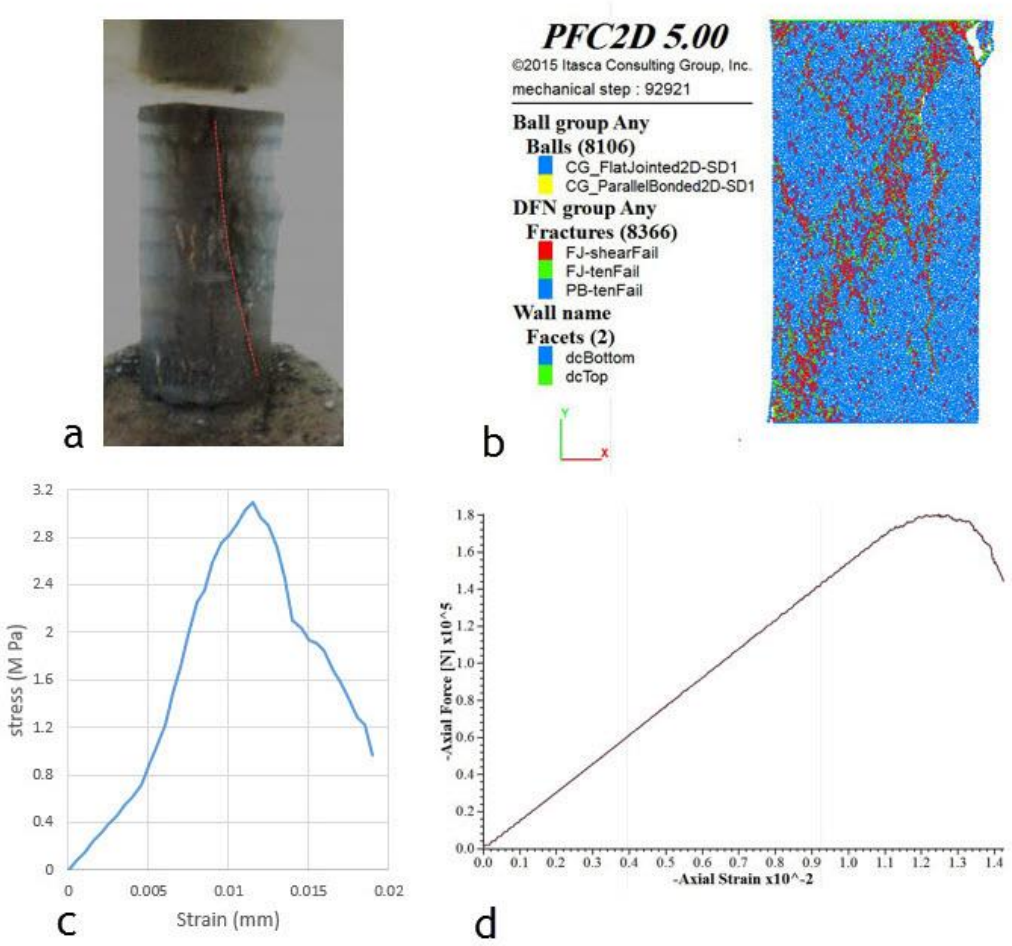


Fig. 21 (a) coal rock failure pattern in experimental UCS test, (b) coal rock failure pattern in numerical UCS test, (c) axial stress versus axial strain in experimental UCS test and (d) axial force versus axial strain in numerical UCS test

distance on the tensile strength. Totally tensile strength was increased by increasing the Particle distance. Its to be note that only when Particle distance was 0.5, the tensile strength and failure pattern was close to experimental one. Therefore the coefficient of 0.5 was chosen for model calibration.

## 4. Comparison between numerical models with experimental results

The numerical model was calibrated when friction angle, Accumulation factor, Expansion coefficient and Particle distance were 20°, 0.7, 1.2 and 0.5 mm, respectively. Table 3 shows micro-parameters used for calibration.

Figs. 21(a) and 21(b) show failure patterns in both of the PFC2D numerical model and experimental sample; respectively. The splitting plane is basically diametrical and it agrees well with the experimental observation. Figs. 21(c) and 21(d) shows the compressive strength versus the axial displacement curve for experimental test and PFC2D numerical UCS test simulation. From Figs. 21(c) and 21(d), it's clear that the bonded particles have a brittle behavior under compressive loading so that they have reached their peak compressive strength and got broken before they get into non-linear deformation stage. The Numerical tensile strength with the comparison of the experimental measurements is presented in Table 4. Table 4 shows that a good accordance was established between experimental test and numerical simulation.

Figs. 22(a) and 22(b) show failure patterns in both of the PFC2D numerical model and experimental sample; respectively. The splitting plane is basically horizontal and it agrees well with the experimental observation. Fig. 22(c) shows the tensile strength versus the axial displacement curve for PFC2D numerical Brazilian simulation. From Fig. 22(c), it's clear that the bonded particles have a brittle behavior under indirect tensile loading so that they have reached their peak tensile strength and got broken before they get into non-linear deformation stage. The Numerical tensile strength with the comparison of the experimental measurements is presented in Table 4. Table 4 shows that a good accordance was established between experimental test and numerical simulation.

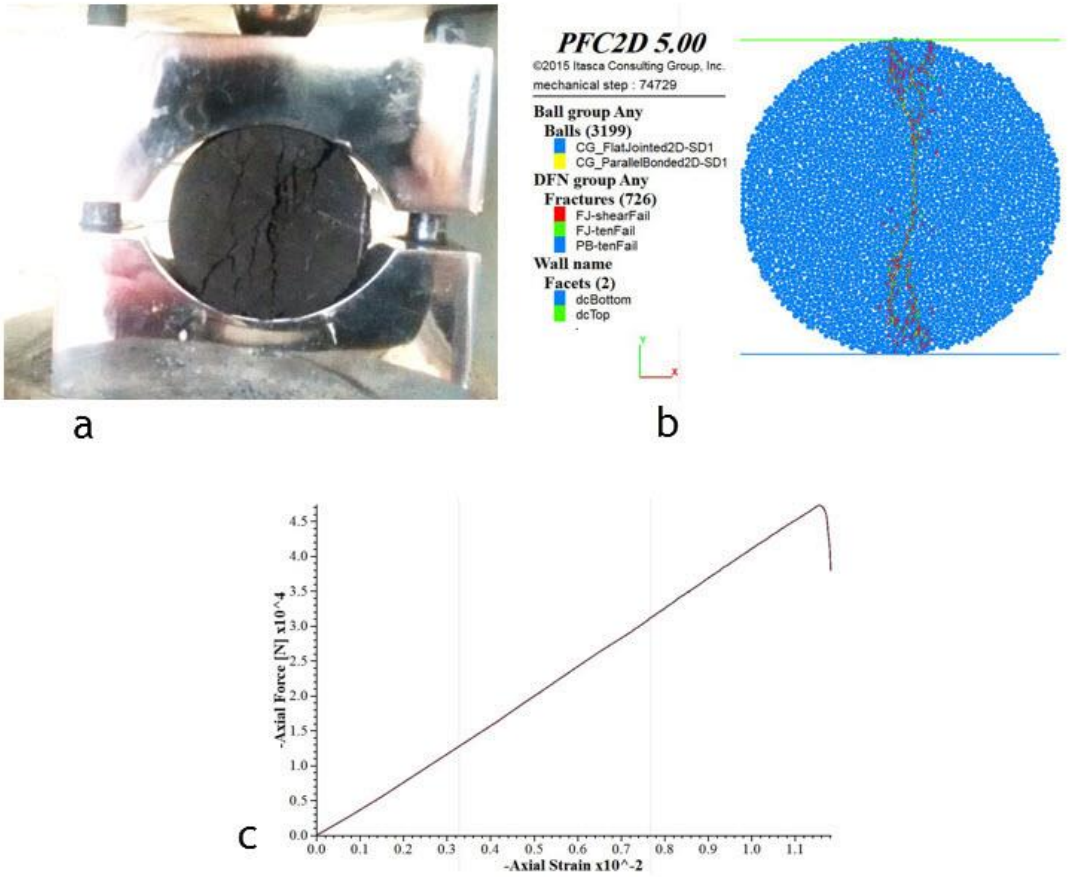


Fig. 22 (a) coal rock failure pattern in experimental brazilian test, (b) coal rock failure pattern in numerical brazilian test and (c) axial force versus axial strain in numerical Brazilian test

Table 3 Micro properties used for model calibration

| No | Micro properties | Value | No | Micro properties | Value |
|---|---|---|---|---|---|
| 1 | Particle distance | 0.5 mm | 11 | Model height | 108 mm |
| 2 | Elastic modulus (yang) | 190 MPa | 12 | Model width | 54 mm |
| 3 | K-ratio | 2 | 13 | Expansion coefficient | 1.2 |
| 4 | Friction coefficient | 0.5 | 14 | Accumulation factor | 0.7 |
| 5 | Tensile strength | 0.85 MPa | 15 | Density | 2500 N/cm$^2$ |
| 6 | Tensile strength standard deviation | 0.001 MPa | 16 | Minimum diameter of particles | 0.6 mm |
| 7 | Compressive strength | 0.7 MPa | 17 | Maximum diameter of particles | 1.2 mm |
| 8 | Compressive strength standard deviation | 0.1 MPa | 18 | Material pressure | 0.1 MPa |
| 9 | Friction angle | 20$^0$ | 19 | Material pressure changes | 0.01 |
| 10 | Porosity | 0.08 | 20 | | |

Table 4 The results of compressive strength and tensile strength rendered by experimental test and numerical simulation

| | Tensile strength (MPa) | Compressive strength (MPa) |
|---|---|---|
| Real value | 0.62 | 3.1 |
| Modeling value | 0.83 | 3.3 |

## 5. Discussion

The output shows that UCS increases by increasing the friction coefficient but tensile strength decrease by increasing the friction coefficient. UCS increases by increasing the accumulative factor but tensile strength decrease by increasing the accumulative factor. UCS increases by increasing the expansion coefficient but tensile strength decrease by increasing the expansion coefficient. UCS and tensile strength were increased by increasing the particle distance.

## 6. Conclusions

The results show that:

- The UCS increase by increasing the friction angle but the tensile strength decreases by increasing the friction angle.
- When brittleness increase its better to choose higher value for friction angle in calibration process.
- Whereas the ratio of uniaxial strength to tensile strength for coal rock is equal to 5, therefore the lower value for friction angle was chosen i.e. 20°. In this friction angel, failure pattern and mechanical properties in numerical simulation were similar to experimental one.
- The UCS increase by increasing the Accumulation factor but the tensile strength decreases by increasing the Accumulation factor. Accumulation factor effect was less than the effect of friction angle.
- Whereas the ratio of uniaxial strength to tensile strength for coal rock is equal to 5, therefore the higher value for Accumulation factor was chosen i.e., 0.7. in this Accumulation factor, failure pattern and mechanical properties in numerical simulation were similar to experimental one.
- The UCS and tensile strength increase by increasing the Expansion coefficient.
- Whereas the ratio of uniaxial strength to tensile strength for coal rock is equal to 5, therefore the lower value for Expansion coefficient factor was chosen i.e., 1.2. in this Expansion coefficient, failure pattern and mechanical properties in numerical simulation were similar to experimental one.
- The UCS and tensile strength increase by increasing the disc distance.
- Whereas the ratio of uniaxial strength to tensile strength for coal rock is equal to 5, therefore the middle value for disc distance was chosen i.e. 0.5 mm. In this disc distance, failure pattern and mechanical properties in numerical simulation were similar to experimental one.
- The calibration of experimental sample was good when model was calibrated by PFC2D version 5.
- By try and error we can calibrate the numerical method.

## References


Akbas, S. (2016), "Analytical solutions for static bending of edge cracked micro beams", *Struct. Eng. Mech.*, **59**(3), 66-78.

Bahaaddini, M., Sharrock, G. and Hebblewhite, B.K. (2013), "Numerical investigation of the effect of joint geometrical parameters on the mechanical properties of a non-persistent jointed rock mass under uniaxial compression", *Comput. Geotech.*, **49**, 206-225, DOI 10.1016/j.compgeo.2012.10.012.

Bahaaddini, M., Hagan, P.C., Mitra, R. and Khosravi, M.H. (2016), "Experimental and numerical study of asperity degradation in the direct shear test", *Eng. Geology*, **204**, 41-52.

Bahrani, N., Valley, B.K. and Kaiser, P. (2015), "Numerical simulation of drilling-induced core damage and its influence on mechanical properties of rocks under unconfined condition", *Int. J. Rock Mech. Min. Sci.*, **80**, 40-50.

Bock, S. and Prusek, S. (2015), "Numerical study of pressure on dams in a backflled mining shaf based on PFC3D code", *Comput. Geotech.*, **66**, 230-244.

Cho, N., Martin, C. and Sego, D. (2007), "A clumped particle model for rock", *Int. J. Rock Mech. Min. Sci.*, **44**(7), 997-1010.

Cundall, P. (1987), Distinct element models of rock and soil structure. (Ed., Brown E.T.) Analytical and computational methods in engineering rock mechanics, Allen & Unwin, London, 129-163

Cundall, P.A. and Strack, O.D.L. (1979), "A discrete numerical model for granular assemblies", *Geotechnique*, **29**(1), 47-65.

Fan, X., Kulatilake, P.H.S.W. and Chen, X. (2015), "Mechanical behavior of rock-like jointed blocks with multi-non-persistent joints under uniaxial loading: a particle mechanics approach", *Eng. Geol.*, **190**, 17-32.

Fan, Y., Zhu, Z., Kang, J. and Fu, Y. (2016), "The mutual effects between two unequal collinear cracks under compression", *Math. Mech. Solids*, **22**, 1205-1218.

Fu, Y. (2005), "Experimental quantification and DEM simulation of micro-macro behaviors of granular materials using X-ray tomography imaging", Ph.D. thesis, Louisiana State University

Gerges, N., Issa, C. and Fawaz, S. (2015), "Effect of construction joints on the splitting tensile strength of concrete", *Case Studies Constr. Mater.*, **3**, 83-91.

Ghazvinian, A., Sarfarazi, V., Schubert, W. and Blumel, M. (2012), "A study of the failure mechanism of planar non-persistent open joints using PFC2D", *Rock Mech. Rock Eng.*, **45**(5), 677-693.

Ghazvinian, E., Kalenchuk, K.S. and Diederichs, M.S. (2017), "Three-dimensional random Voronoi models for simulation of brittle rock damage around underground excavations in laminated ground", Deep Mining, Perth, Australia.

Haeri, H. (2015), "Simulating the crack propagation mechanism of pre-cracked concrete specimens under shear loading conditions", *Strength Mater.*, **47**(4), 618-632.

Haeri, H. and Sarfarazi, V. (2016a), "The effect of non-persistent joints on sliding direction of rock slopes", *Comput. Concrete*, **17**(6), 723-737.

Haeri, H., Khaloo, A. and Marji, M.F. (2015a), "Fracture analyses of different pre-holed concrete specimens under compression", *Acta Mech. Sinic.*, **31**(6), 855-870.

Haeri, H., Khaloo, A. and Marji, M.F. (2015b), "A coupled experimental and numerical simulation of rock slope joints behavior", *Arab. J. Geosci.*, **8**(9), 7297-7308.

Haeri, H., Sarfarazi, V. and Lazemi, H. (2016), "Experimental study of shear behavior of planar non-persistent joint", *Comput. Concrete*, **17**(5), 639-653.

Haeri, H. and Sarfarazi, V. (2016b), "The effect of micro pore on the characteristics of crack tip plastic zone in concrete", *Comput. Concrete*, **17**(1), 107-127.

Haeri, H., Shahriar, K. and Marji, M.F. (2013), "Modeling the propagation mechanism of two random micro cracks in rock samples under uniform tensile loading", *Proceedings of the ICF13*.

Hofmann, H., Babadagli, T., Yoon, J.S., Blöcher, G. and Zimmermann, G. (2016), "A hybrid discrete/finite element modeling study of complex hydraulic fracture development for enhanced geothermal systems (EGS) in granitic basements", *Geothermics*, **64**, 362-381.

Hofmann, H., Babadagli, T., Yoon, J.S., Zang, A. and Zimmermann, G. (2015), "A grain based modeling study of mineralogical factors affecting strength, elastic behavior and micro fracture development during compression tests in granites", *Eng. Fract. Mech*,, **147**, 261-275.

Huang, H. (1999), "Discrete element modeling of tool-rock interaction", Ph.D. thesis, University of Minnesota, Minneapolis, MN

Imani, M., Nejati, H.R. and Goshtasbi, K. (2017), "Dynamic response and failure mechanism of Brazilian disk specimens at high strain rate", *Soil Dyn. Earthq. Eng*., **100**, 261-269.

Jing, L. (2003), "A review of techniques, advances and outstanding issues in numerical modelling for rock mechanics and rock engineering", *Int. J. Rock Mech. Min. Sci*., **40**(3), 283-353. doi:10. 1016/s1365-1609(03)00013-3

Jong, Y.H. and Lee, C.G. (2006), "Suggested method for determining a complete set of micro-parameters quantitatively in PFC2D", *Tunn. Undergr. Sp*., **16**(4), 334-346.

Khazaei, C., Hazzard, J. and Chalaturnyk, R. (2015), "Damage quantifcation of intact rocks using acoustic emission energies recorded during uniaxial compression test and discrete element modeling", *Comput. Geotech*., **67**, 94-102.

Khodayar, A. and Nejati, H.R.(2018), "Effect of thermal-induced microcracks on the failure mechanism of rock specimens", *Comput. Concrete*, **22**(1), 93-100.

Kim, H.M., Lee, J.W., Yazdani, M., Tohidi, E., Nejati, H.R. and Park, E.S. (2018), "E.-S coupled viscous fluid flow and joint deformation analysis for grout injection in a rock joint", *Rock Mech. Rock Eng.*, **51**(2), 627-638.

Koyama, T. and Jing, L. (2007), "Effects of model scale and particle size on micro-mechanical properties and failure processes of rocks—a particle mechanics approach", *Eng. Anal. Bound. Elem*., **31**(5), 458-472.

Lancaster, I.M., Khalid, H.A. and Kougioumtzoglou, I.A. (2013), "Extended FEM modelling of crack propagation using the semi-circular bending test", *Constr. Build. Mater*., **48**, 270-277.

Lee, H., Moon, T. and Haimson, B.C. (2016), "Borehole breakouts induced in Arkosic sandstones and a discrete element analysis," *Rock Mech. Rock Eng*., **49**(4), 1369-1388.

Lee, S. and Chang, Y. (2015), "Evaluation of RPV according to alternative fracture toughness requirements", *Struct. Eng. Mech*., **53**(6), 1271-1286.

Li, X., Wang, S.H., Malekian, R., Hao, S.H. and Li, Z.H. (2016), "Numerical simulation of rock breakage modes under confining pressures in deep mining: An experimental investigation", IEEE Access, Digital Object Identifier 10.1109/ACCESS.2016.2608384.

Li, S.H., Li, D., Cao, L. and Shangguan, Z. (2014), "Parameter estimation approach for particle flow model of rockfill materials using response surface method", ICCM, 28-30th July, Cambridge, England.

Li, S., Wang, H., Li, Y., Li, Q., Zhang, B. and Zhu, H. (2016), "A new mini-grating absolute displacement measuring system for static and dynamic geomechanical model tests", *Measurement*, **82**, 421-431.

Lin, C.H. and Lin, M.L. (2015), "Evolution of the large landslide induced by Typhoon Morakot: a case study in the Butangbunasi River, southern Taiwan using the discrete element method", *Eng. Geol.*, **197**, 172-187.

Liu, X., Nie, Z., Wu, S. and Wang, C. (2015), "Self-monitoring application of conductive asphalt concrete under indirect tensile deformation", *Case Studies Constr. Mater*., **3**, 70-77.

Lu, F.Y., Lin, Y.L., Wang, X.Y., Lu, L. and Chen, R. (2015), "A theoretical analysis about the influence of interfacial friction in SHPB tests", *Int. J. Impact Eng*., **79**, 95-101.

Mehranpour, M.H., Kulatilake, P.H.S.W. (2016), "Comparison of six major intact rock failure criteria using a particle flow approach under true-triaxial stress condition", *Geomech. Geophys. Geo-Energy Geo-Resources*, **2**, 203-229.

Mobasher, B., Bakhshi, M and Barsby, C. (2014), "Backcalculation of residual tensile strength of regular and high performance fibre reinforced concrete from flexural tests", *Constr. Build. Mater*., **70**, 243-253, 2014.

Mohammad, A. (2016), "Statistical flexural toughness modeling of ultra-high performance mortar using response surface method", *Comput. Concrete*, **17**(4), 33-39.

Morgan, S., Johnson, A.A. and Einstein, H.H. (2013), "Cracking processes in Barre granite: fracture process zones and crack coalescence", *Int. J. Fracture*, **180**, 177-204.

Najigivi, A., Nazerigivi, A. and Nejati, H.R. (2017), "Contribution of steel fiber as reinforcement to the properties of cement-based concrete: A review", *Comput. Concrete*, **20**(2), 155-164.

Nazerigivi, A., Nejati, H.R., Ghazvinian, A. and Najigivi, A. (2018), "Effects of SiO2 nanoparticles dispersion on concrete fracture toughness", *Constr. Build. Mater*., **171**(20), 672-679.

Noel, M. and Soudki, K. (2014), "Estimation of the crack width and deformation of FRP-reinforced concrete flexural members with and without transverse shear reinforcement", *Eng. Struct*., **59**, 393-398.

Oetomo, J.J., Vincens, E., Dedecker, F. and Morel, J.C. (2016), "Modeling the 2D behavior of dry-stone retaining walls by a fully discrete element method", *Int. J. Numer. Anal. Meth. Geomech*., **40**(7), 1099-1120.

Oliaei, M. and Manaf, E. (2015), "Static analysis of interaction between twin-tunnels using discrete element method (DEM)", *Scientia Iranica*, **22**(6), 1964-1971.

Oliveira, H.L. and Leonel, E.D. (2014), "An alternative BEM formulation, based on dipoles of stresses and tangent operator technique, applied to cohesive crack growth modeling", *Eng. Anal. Bound. Elem*., **41**, 74-82.

Pan, B., Gao, Y. and Zhong, Y. (2014), "Theoretical analysis of overlay resisting crack propagation in old cement mortar pavement", *Struct. Eng. Mech*., **52**(4), 167-181.

Potyondy, D.O. and Cundall, P.A. (2004), "A bonded-particle model for rock", *Int. J. Rock Mech. Min. Sci*., **41**(8), 1329-1364. doi:10.1016/j. ijrmms.2004.09.011

Potyondy, D. (2015), Material-Modeling Support in PFC 2015. Itasca Consuling Groupe, Inc.

Potyondy, D. and Cundall, P. (2004), "A bonded-particle model for rock", *Int. J. Rock Mech. Min. Sci*., **41**, 1329-1364.

Rajabi, M., Soltani, N. and Eshraghi, I. (2016), "Effects of temperature dependent material properties on mixed mode crack tip parameters of functionally graded materials", *Struct. Eng. Mech.*, **58**(2), 144-156.

Ramadoss, P. and Nagamani, K. (2013), "Stress-strain behavior and toughness of high-performance steel fiber reinforced mortar in compression", *Comput. Mortar*, **11**(2), 55-65.

Sardemir, M. (2016), "Empirical modeling of flexural and splitting tensile strengths of concrete containing fly ash by GEP", *Comput. Concrete*, **17**(4), 489-498.

Sarfarazi, V., Haeri, H. and Khaloo, A. (2016b), "The effect of non-persistent joints on sliding direction of rock Slopes", *Comput. Concrete*, **17**(6), 723-737.

Sarfarazi, V., Ghazvinian, A., Schubert, W., Blumel, M. and Nejati, H.R. (2014), "Numerical simulation of the process of fracture of

echelon rock joints", *Rock Mech. Rock Eng*., **47**(4), 1355-1371.
Sarfarazi, V. and Haeri, H. (2016a), "Effect of number and configuration of bridges on shear properties of sliding surface", *J. Min. Sci*., **52**(2), 245-257.
Sarfarazi, V., Haeri, H. and Khaloo, A. (2016), "The effect of non-persistent joints on sliding direction if rock slopes", *Comput. Concrete*, **17**(6)**,** 723-737.
Shuraim, A.B., Aslam, F., Hussain, R. and Alhozaimy, A. (2016), "Analysis of punching shear in high strength RC panels–experiments, comparison with codes and FEM results", *Comput. Concrete*, **17**(6), 739-760.
Silva, R.V., Brito, J. and Dhir. R.K. (2015), "Tensil strength behaviour of recycled aggregate concrete", *Constr. Build. Mater*., **83**, 108-118.
Tiang, Y., Shi, S., Jia, K. and Hu, S. (2015), "Mechanical and dynamic properties of high strength concrete modified with lightweight aggregates presaturated polymer emulsion", *Constr. Build. Mater*., **93**, 1151-1156.
Turichshev, A. and Hadjigeorgiou, J. (2015), "Experimental and numerical investigations into the strength of intact veined rock", *Rock Mech. Rock Eng.*, **48**(5), 1897-1912.
Vallejos, J.A., Suzuki, K., Brzovic, A. and Ivars, D.M. (2015), "Application of synthetic rock mass modeling to veined core-size samples", *Int. J. Rock Mech. Min. Sci.*, **81**, 47-61,
Wan Ibrahim, M.H., Hamzah, A.F., Jamaluddin, N., Ramadhansyah, P.J. and Fadzil, A.M. (2015), "Split tensile strength on self-compacting concrete containing coal bottom ash", *Procedia - Social and Behavioral Sciences*, **198**, 2280-2289.
Wang, M. and Cao, P. (2017), "Calibrating the micromechanical parameters of the PFC2D(3D) models using the improved simulated annealing algorithm", *Math. Probl. Eng*.
Wang, P., Yang, T., Xu, T., Cai, M. and Li, C. (2016), "Numerical analysis on scale effect of elasticity, strength and failure patterns of jointed rock masses", *Geosci. J*., **20**(4), 539-549.
Wang, Y. and Tonon, F. (2009), "Modeling Lac du Bonnet granite using a discrete element model", *Int. J. Rock Mech. Min. Sci*., **46**(7), 1124-1135
Wang, Y. and Tonon, F. (2010), "Calibration of a discrete element model for intact rock up to its peak strength", *Int. J. Numer. Anal. Method. Geomech*., **34**(5), 447-469. doi:10.1002/nag.811
Wang, Z., Jacobs, F. and Ziegler, M. (2016), "Experimental and DEM investigation of geogrid-soil interaction under pullout loads", *Geotextiles and Geomembranes*, **44**(3), 230-246.
Wang, T., Dai, J.G. and Zheng, J.J. (2015), "Multi-angle truss model for predicting the shear deformation of RC beams with low span-effective depth ratios", *Eng. Struct*., **91**, 85-95.
Wang, X., Zhu, Z., Wang, M., Ying, P., Zhou, L. and Dong, Y. (2017), "Study of rock dynamic fracture toughness by using VB-SCSC specimens under medium-low speed impacts", *Eng. Fract. Mech*., **181**, 52-64.
Wen, Z.J., Wang, X. and Li, Q.H. (2016), "Simulation analysis on the strength and acoustic emission characteristics of jointed rock mass", *Technical Gazette*, **23**(5), 1277-1284.
Wu, Z.J., Ngai, L. and Wong, Y. (2014), "Investigating the effects of micro-defects on the dynamic properties of rock using numerical manifold method", *Constr. Build. Mater*., **72**, 72-82
Yan, Y. and Ji, S, (2010), "Discrete element modeling of direct shear tests for a granular material", *Int. J. Numer. Anal. Meth. Geomech*., **34**(9), 978-990. doi:10.1002/nag.848
Yang, S.Q., Tian, W.L., Huang, Y.H., Ranjith, P.G. and Ju, Y. (2016), "An experimental and numerical study on cracking behavior of brittle sandstone containing two non-coplanar fssures under uniaxial compression", *Rock Mech. Rock Eng*., **49** (4), 1497-1515.
Yang, X., Kulatilake, P.H.S.W., Jing, H. and Yang, S. (2015), "Numerical simulation of a jointed rock block mechanical behavior adjacent to an underground excavation and comparison with physical model test results", *Tunn. Undergr. Sp. Tech.*, **50**, 129-142.
Yao, W., Hu, B., Li, L., Chen, X. and Rao, C.H. (2016), "Particle flow simulation of the direct shear tests on the weak structural surface", *Electronic J. Geotech. Eng*., 21.
Yaylac, M. (2016), "The investigation crack problem through numerical analysis", *Struct. Eng. Mech.*, **57**(6).
Yoon, J. (2007), "Application of experimental design and optimization to PFC model calibration in uniaxial compression simulation", *Int. J. Rock Mech. Min. Sci*., **44**, 871-889
Zhang, Q., Zhu, H., Zhang, L. and Ding, X. (2011), "Study of scale effect on intact rock strength using particle flow modeling", *Int. J. Rock Mech. Min. Sci*., **48**(8), 1320-1328. doi:10.1016/j.ijrmms.2011.09.016
Zhang, Q., Zhu, H.H. and Zhang, L. (2015), "Studying the effect of non-spherical micro-particles on Hoek-Brown strength parameter mi using numerical true triaxial compressive tests", *Int. J. Numer. Anal. Meth. Geomech.*, **39**(1), 96-114.
Zhang, X.P. and Wong, L. (2012), "Cracking processes in rock-like material containing a single flaw under uniaxial compression: a numerical study based on parallel bonded-particle model approach", *Rock Mech. Rock Eng*., **45**(5), 711-737. doi:10.1007/s00603-011-0176-z
Zhao, Y., Zhao, GF. and Jiang, Y. (2013), "Experimental and numerical modelling investigation on fracturing in coal under impact loads", *Int. J. Fracture*, **183**(1), 63-80.
Zhou, M. and Song, E. (2016), "A random virtual crack DEM model for creep behavior of rockfll based on the subcritical crack propagation theory", *Acta Geotech*., **11**(4), 827-847.

*CC*

`